Volume 1 | Number 1 | Jan 2013 | Pages 1–100

Journal of
Materials Chemistry A

Materials for energy and sustainability
www.rsc.org/materialsA

Li⁺

ROYAL SOCIETY
OF CHEMISTRY

ROYAL SOCIETY
OF CHEMISTRY

www.rsc.org/materialsA

Efficient Hydrogen/Oxygen Evolution and Photocatalytic Dye Degradation and Reduction of Aqueous Cr(VI) by Surfactant Free Hydrophilic Cu$_2$ZnSnS$_4$ Nanoparticles

Priya Kush, Kalyanjyoti Deori, Anup Kumar and Sasanka Deka*

Department of Chemistry, University of Delhi, North Campus, Delhi-110007, India

E. mail: sdeka@chemistry.du.ac.in, ssdeka@gmail.com

Abstract. A single type of semiconductor material, surfactant free hydrophilic Cu$_2$ZnSnS$_4$ (CZTS) nanoparticles for the first time has been explored as three way heterogeneous catalysts in electrocatalytic hydrogen evolution reaction (HER), photocatalytic degradation of polluting dyes and photocatalytic reduction of carcinogenic and mutagenic Cr (VI) to nontoxic Cr (III). Ultrafine surfactant free nanoparticles of kesterite CZTS (~4 nm) having optimum band gap of 1.75 eV and electrical resistivity of 0.6 Ω.m was used for the demonstrated applications. The as-synthesized CZTS NPs showed promising electrocatalytic activity for HER as well as oxygen evolution reaction (OER) with lower Tafel slope and excellent recyclable catalytic efficiency. Rhodamine B, Methyl Red and Methylene Blue dyes have been degraded rapidly and efficiently in a photocatalytic pathway by the as-synthesized CZTS nanoparticles, where only 5% activity loss in degradations after 10th cycles. Similarly, higher rate constant and activity parameter were observed for the photocatalytic reduction of hexavalent chromium ions. The high catalytic performance of present CZTS NPs over the other catalysts under indoor light condition in absence of any expensive noble metal and harsh reducing/oxidizing agent have been attributed to size, surface charge and electronic effect.

Keywords: kesterite Cu$_2$ZnSnS$_4$; nanoparticles; hydrogen evolution; oxygen evolution; photocatalyst.

1. Introduction

Semiconductors and their nanocomposite with noble metals, carbon allotropes and polymers have wide range of advanced applications including energy harvesting and energy storage, catalytic applications for many commercially important reactions, biological applications as in sensors and drug delivery etc.[1-5] A multifunctional material that shows more than one properties becomes all the more important for powerful technological applications.[6-

1

[8] In the same scenario if a multifunctional semiconductor nanoparticle (NP) shows more than two potential applications, that material will have a huge impact in economy and environment. Quaternary multivalent Cu_2ZnSnS_4 with high absorption coefficient, optimum direct band gap (1.4-1.6 eV) has been explored well for photovoltaic applications.[9,10] But apart from harvesting sunshine, the quaternary chalcogenides have recently gained interest for thermoelectric as well as photocatalytic applications that revealed the multifunctional aspects of the material.[3,11,12] The challenging task of maintaining stoichiometry, homogeneity and reproducibility in these complex quaternary materials have also been overcome with advancement in synthetic procedures. Also the surfactant free nanomaterials synthesized with advanced synthetic procedures possibly help in realizing the demanding but low cost crucial applications.[13-15] Thus Cu_2ZnSnS_4 could be a potential low cost multifunctional material in the first instance, if we can prove additional important usability of this material such as in electrocatalytic water splitting for H_2/O_2 evolution, photocatalytic redox reactions, etc. apart from their thermoelectric and photovoltaic applications.

Although platinum is the most electroactive and efficient catalyst for hydrogen evolution reaction at low overpotentials, however this noble metal is neither operationally cost effective nor sufficient in context of HER catalysis at a scale comparable to the global energy demand. In the replacement of costly metal catalysts, several other metal chalcogenides or oxides applicable at comparatively lower overpotential have been greatly introduced in recent years.[16-19] However, problems like lesser number of active sites, poor electrical transport, inefficient electrical contact to the catalyst and instability under operating conditions, etc. are modified for an enhanced rate constant by the chemical exfoliation or functionalization either by compounds having high surface area or which can enhance the active reaction sites.[20-22] However, chemical exfoliation or surface modification techniques for these compounds are not preparation effective and performed under harsh reaction condition, which makes electrocatalyst's preparation and study complicated and much lengthy.[21] CZTS, a low cost photovoltaic material is a promising *p*-type semiconductor which has been investigated recently in photocatalytic water splitting reaction and efficiently produced H_2 from water.[12] But electrochemical behaviours of CZTS on HER and OER activity are still not known and yet to be explored.

On the other hand removal of confirmed carcinogenic and mutagen Cr(VI) from waste water body or its reduction to nontoxic Cr(III), and degradation of polluting organic dyes present in industrial waste water is challenging task and topic of current research. Various

2

attempts have been made to outperform the photocatalytic activity of TiO_2 by means of development of new environmentally benign and viable materials for the destructive oxidation of recalcitrant pollutant organic dye molecules.[3,23-26] Organic dyes such as methyl orange, Rhodamine B, methylene blue, methyl red, Eosin Y, etc., which are generally used in dye industries, textile industries and biological tagging cause adverse effect on our environment, so their degradation is necessary before discharging them to aquatic environment. Literature reveals that, a 3 mg/L solution of Cr(VI) fully photocatalyzed by commercial TiO_2 (Degussa P25) in less than 0.5 h under UV irradiation and commercial TiO_2 (Hombikat UV100) took 4 h for the same reduction reaction.[27] Whereas, an acidic medium was found favorable for Cr(VI) photocatalytic reduction, where 94% of Cr(VI) was photoreduced within 1 h at pH 3 when 2 g/L of TiO_2 was used as the slurry.[28] Recently, high energy electron beam (HEEB) irradiation was used to disperse nanoscale zero-valent iron (NZVI) for reduction of Cr(VI) to Cr(III) in aqueous solution.[29] Cu_2ZnSnS_4 NPs could be an alternative to the above mentioned photocatalyst due to its intrinsic high optical absorption coefficient and optimum direct band gap.

Herein, as a foremost case, we report surfactant free hydrophilic nanocrystalline CZTS synthesized via hydrothermal method as highly efficient electrocatalyst for hydrogen evolution reaction, oxygen evolution reaction (OER) as well as photocatalyst for the degradation of variety of carcinogenic pollutant dyes (Rhodamine B, RhB; Methylene blue, MB and Methyl Red, MR) and photocatalytic reduction of confirmed carcinogen Cr(VI) under indoor illumination. Surfactant free CZTS nanopartices were chosen for the study to avoid any tedious and costly surfactant removal or exchange process and used as multifunctional three way heterogeneous catalyst. The same material first acts as oxidizing catalyst in the electrochemical water splitting reactions and then photocatalytic dye degradation reactions, and later acts as reducing catalyst in the Cr(VI) reduction reactions. Heterogeneous photocatalytic degradation of carcinogenic pollutants dyes from waste water and reduction of carcinogenic Cr(VI) under indoor light illumination without incorporation of any expensive noble metal, in the absence of any harsh reducing/oxidizing agent and scavenger or sacrificial electron acceptor; and artificial UV radiation is highly efficient and economical.

2. Experimental section

2.1. Chemicals: Copper (II) chloride dihydrate ($CuCl_2.2H_2O$, 99%) and Zinc chloride ($ZnCl_2$, 95%) were purchased from Merck India. Tin (II) chloride dihydrate ($SnCl_2.2H_2O$, 98%), Rhodamine B (97%), Eosin Y (~99%) were purchased from Sigma Aldrich, USA; and

sodium sulfide nonahydrate (Na$_2$S.9H$_2$O, 55-58%) were purchased from Thomas Baker, India. Methylene Blue and Methyl Red was purchased from Spectrochem, India. Potassium dichromate (K$_2$Cr$_2$O$_7$, 99.9%) was purchased from Qualigen Fine Chemicals, India. All the chemicals were used as received without further purification.

2.2. Synthesis of Cu$_2$ZnSnS$_4$ nanoparticles: Hydrothermal synthesis method has been used to synthesize Cu$_2$ZnSnS$_4$ nanocrystals without using any surfactants as reported in our earlier work.[14] In a typical synthesis, CuCl$_2$.2H$_2$O (0.170g, 1 mmol) was dissolved in distilled water (40 ml). SnCl$_2$.2H$_2$O (0.112g, 0.5 mmol) and ZnCl$_2$ (0.136g, 1 mmol) were added to the above solution while stirring. The solution was then ultrasonicated for 10 minutes to form a homogenous solution. Na$_2$S.9H$_2$O (0.480g, 2 mmol) was then added followed by stirring of additional 5 minutes to form a brown-black mixture. The mixture was then transferred to a 50 ml Teflon lined hydrothermal flask and heated at 180 ^{0}C for 18 hrs in a temperature controlled oven and then allowed to cooled down to room temperature naturally. The black product was collected and washed with distilled water and ethanol three times. The obtained product was dried at 60 ^{0}C for 4 hrs and stored for further use.

2.3. Instrument details: Powder X-ray diffraction (PXRD) measurements were performed with Bruker D8 discover X-ray diffractometer employing monochromatized Cu Kα radiation (λ = 1.54056 Å) at 298 K. Low resolution transmission electron microscopy (TEM) images, phase-contrast high-resolution TEM (HRTEM) images and selected area electron diffraction (SAED) measurements were performed with a Philips Technai G^{2}30 transmission electron microscope operating at an accelerating voltage of 200 kV. Optical absorption measurements were carried out using a Perkin-Elmer Lambda 35 UV-Vis spectrophotometer. Nanocrystals were dispersed either in water or ethanol for this purpose. The electrochemical studies were performed on CHI 660D potentiostat. Brunauer–Emmett–Teller (BET) surface area analysis was performed on powder sample with Micromeritics Instrument Corp. (USA) Gemini V2. DLS studies were carried out using a Zeta sizer Nano-ZS. High resolution X-ray photoelectron spectroscopy (XPS) was performed with a Multitechnique surface analysis system from Omicron Nanotechnology equipped with a monochromatic radiation source (AlKa, 1486.6 eV) and hemispherical analyzer (resolution 0.6 eV) under a vacuum of 10^{-1} mbar and 225 W.

2.4. Electrocatalytic HER/OER measurements: Finely ground 30 mg CZTS powder was taken in a solution of 5 wt % nafion (0.3 mL) in 3 mL ethanol (nafion to ethanol ratio: 1:10) and mixed ultrasonically for 30 min to obtain a ink type suspension. So obtained suspension

was drop-casted onto a glassy carbon electrode of 4 mm diameter. These deposited thin films were dried at 40 °C overnight and used as working electrodes. Cyclic Voltammetry (CV), linear sweep voltametry (LSV) and electrochemical impedance spectroscopy (EIS) were performed on a three electrode cell with a loading density of 15.6 mg/cm^2 on single electrode. CV, LSV and EIS measurements were performed (CHI 660D potentiostat) with scan rate ranging from 10 to 20 mV s^{-1} in 0.5 M H$_2$SO$_4$ solution using Ag/AgCl (1M KCl) as the reference electrode and a graphite rod as the counter electrode. Electrolyte was degassed by bubbling N$_2$ for 30 min prior to the start of each experiment. The electrochemical impedance spectroscopy (EIS) measurements were carried out in the same configuration at overpotential $\eta = 120$ mV from 10^6 to 0.02 Hz with an AC voltage of 5 mV.

2.5. Photocatalytic dye degradation measurements: All photocatalytic measurements have been carried out considering the factors recently reported by Buriak *et al.*[30] In a typical photocatalytic reaction 50 ml of dye solution in the concentration range 0.002−0.01 mM was added into a beaker containing 10−25 mg of the hydrophilic CZTS nanocatalyst, depending on reactions. The solution was sonicated for 10 s for the complete dispersion of CZTS catalyst followed by continuous stirring under indoor illumination. 1 ml of the solution was taken out at various time intervals and centrifuged at 4000 rpm and then optical absorption measurements were performed on the decanted liquid. For the illumination purpose, a commercial TL5 high efficiency mercury-vapor gas-discharge lamp or fluorescent lamp (40 W, 2450 lumens) was used as the light source and the wavelength distribution of the light source is 400-700 nm (white light). Distance between the light source and the reaction beaker is 3 m and the optical irradiance at the sample position is measured using a solar meter to be 0.08 mW/cm^2. The photo degradation efficiency of the as-synthesized CZTS sample was calculated as:

$$\text{Catalytic degradation efficiency (\%)} = \text{percentage dye degradation} = \frac{A_0 - A_t}{A_0}.100 \qquad (1)$$

where, A$_o$ is the initial absorbance before the addition of catalyst and A$_t$ is the absorbance at time '*t*' after the addition of catalyst. The reaction rate constant '*k$_{app}$*' was determined by utilizing the following equation assuming the reaction to follow first order kinetics.

$$\text{In}[A_t][A_o] = -k_{app}t \qquad (2)$$

In all cases catalytic degradation efficiency is ultimate, as there is no contribution of light absorption from the photocatalyst since the photocatalyst was removed by centrifugation prior to optical absorbance measurements.

2.6. Cr(VI) reduction study: In a typical photocatalytic Cr(VI) reduction reaction, 50 ml of $K_2Cr_2O_7$ solution in the concentration range 0.01−0.1 mM was added into a beaker containing 25-50 mg of the hydrophilic bare CZTS nanocatalyst. The solution was kept for continuous stirring under identical illumination as mentioned in the case of dye degradation. 1 ml of the solution was taken out at various time intervals and centrifuged at 4000 rpm and then optical absorption measurements were performed on the decanted liquid.

2.7. Catalyst reproducibility and stability: Initially the as-synthesized surfactant free CZTS NPs sample was checked for stability by performing XRD measurements on aged samples (stored up to 1 month) before performing catalytic reactions. All catalytic reactions were repeated several times with varied amount of catalyst and concentration of substrates. Water splitting reactions were studied for 100 catalytic cycles with same CZTS working electrode without any further modification. Dye degradation and reduction of Cr(VI) is carried out for up to 25 times with reused CZTS catalyst to check the reproducibility of the obtained results. Catalyst samples were recovered, dried and reused to check the reusability of the samples.

3. Results and Discussion

The synthesis protocol followed for the synthesis of surfactant free CZTS nanoparticles is taken from our earlier report.[14] The new material characterization results are shown in Fig. 1. The environmentally friendly, ~4 nm ultrafine particles (obtained from histogram graph) are stable in water and there was no secondary impurity phase present as corroborated by powder XRD, Raman spectrum, HRTEM imaging and SAED pattern as shown in Fig. 1a-d and Fig. 1e,f. These results are consistent with our previous report[14] on the synthesis and characterization of the as-synthesized material. The reticular (112) planes of kesterite CZTS particle could be clearly characterize from the well-defined lattice fringes as seen in panel 'e' under HRTEM analysis (more image in Fig. S1, ESI). Moreover the as-synthesized sample shows higher absorption across the visible and near-infrared spectral regions and a band gap E_g of 1.75 eV for the as-synthesized sample which is blue shifted as compared to the bulk value due to the nanosized confinement effect (Fig. 1g). Furthermore, the electrical resistivity, 0.6 Ω.m at 300 K is of as-synthesized CZTS could be crucial for electrocatalytic applications.[14]

3.1. Electrocatalytic Water Splitting (HER and OER)

The as-synthesized CZTS ink has been explored as an effective electrochemical catalyst for the hydrogen and oxygen evolution reaction for the first time and the obtained results are

displayed in Fig. 2. Electrochemical characterization and the activity of our CZTS catalyst is evaluated in a typical three electrode cell setup with different H_2SO_4 electrolyte concentration viz., 1M and 0.5 M with CZTS nanoparticles deposited on glassy carbon (GC) electrode employed as the working electrode. The observed non-Faradaic current as well as non-cyclic behavior of CV curve in 0.5 M KOH electrolyte implies the ineffectiveness of CZTS in the basic condition. Therefore we have chosen the acidic media for all electrochemical performances. As shown in Fig. 2a the cyclic voltammogram (CV) of CZTS nanoparticles ink produced by hydrothermal method on GC has substantial HER activity, while the HER current density of the pure GC catalyst is negligible by comparison. It can clearly be seen from the polarization curve that a higher current density of -15.9 mA.cm^{-2} was observed when 0.5 M concentration of H_2SO_4 electrolyte was used while -9.8 mA.cm^{-2} current density was observed in 1M electrolyte. Thus 0.5 M H_2SO_4 was considered for further analysis. The current densities in this study using glassy carbon electrode are comparable with single MoS_2 nanoparticles and even higher than copper metal nanoparticles reported recently,[17,20] which indicates that CZTS could be a promising alternative in near future for electrocatalytic hydrogen evolution reaction. All electrochemical characterizations for HER activity were carried out in a potential range between 0.0 V and -1.5 V (vs. Ag/AgCl) with a scan rate of 10 mV.sec^{-1}, which was set by operating CV at different scan rate (inset of Fig. 2c), and catalyst stability was measured by observing change of current density during 100 potential cycles. The CV of CZTS catalyst in Fig. 2b was stable without significant change in shape, indicating excellent cycling stability of the as-synthesized CZTS in acidic solution. The activity loss was found to be only 11.8% after 100 catalytic cycles (inset, Fig. 2b). The higher value of cathodic current at -1.5 V is associated with the evolution of hydrogen on the hydrophilic CZTS nanoparticles. The higher activity is due to pure hydrophilic nature of our as synthesized electrocatalyst, better stability in acidic medium, absence of any surfactant and smaller particle size. The possible cathodic hydrogen evolution reaction steps on CZTS catalyst in acidic medium can be expressed as follows:[18]

$$CZTS + H_3O^+ + e^- \rightarrow H_{ads}CZTS + H_2O \tag{3}$$

$$H_{ads}CZTS + H_3O^+ + e^- \rightarrow H_2 + H_2O \tag{4}$$

$$H_{ads}CZTS + H_{ads}CZTS \rightarrow H_2 + 2CZTS \tag{5}$$
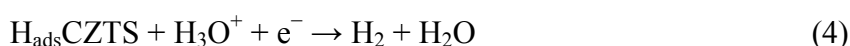
The reaction kinetics of HER was further studied by measuring the Tafel slope which is an inherent property of the catalyst from overpotential versus log current density (η vs log i) plot as shown in Fig. 2c. Tafel analysis of polarization measurements of CZTS on glassy carbon

electrode yielded a Tafel slope of 52 mV.dec^{-1} in 0.5 M H$_2$SO$_4$ which suggest the Volmer−Heyrovsky reaction mechanism responsible for HER in our case. This Tafel slope value nearly corresponds to Heyrovsky reaction which is desorption step here and hence after an electrochemical step which involves a fast discharge of a proton, desorption of hydrogen from adsorbed catalyst is the rate determining step.[31] The lower Tafel slope obtained in the present case is very near to values reported for CoP/Ti[32] and MoS$_2$/RGO[20] etc. suggesting our CZTS a better candidate for electrode in HER without any support. This could be due to vectorial transfer of electrons from negatively charged surface of CZTS nanoparticles, which can then act as a driving force to reduce the electrochemical resistance. The electrode kinetics of CZTS/GC in HER from electrochemical impedance spectroscopy (EIS) also further revealed that the as-synthesized nanoparticles exhibit more facile electrode kinetics, which is a very useful feature in enhancing the catalytic activity. The Nyquist plots of the sample in different electrolyte concentration are depicted in Fig. 2d. From Fig. 2d charge transfer resistance (R_{CT}) for CZTS catalyst in 0.5M electrolyte was found to be 37 Ω from semicircle of Nyquist plot. This lower R_{CT} value corresponds to a faster reaction rate and thus could contribute to the superior electrocatalytic activity. The CZTS nanoparticles had a measured Brunauer–Emmett–Teller (BET) surface area of 15.0 m^{2}g^{-1} (see Fig. S2 for BET curve). Using this surface area, the turnover frequency[32] (TOF) was calculated to be 0.03 s^{-1} at $\eta =$ 1.5 V; and 0.0037 s^{-1} at $\eta = 900$ mV, respectively (see Supporting Information for detailed calculations). Further, the exchange current density (i) was calulated to get an impresion on the charge transfer resistance bahavior of the working electrode. The calculated i value 2.76 mA.cm^{-2} implied a lower charge transfer resistance at the electrode interface (see ESI for calculations).

Oxygen evolution reaction was also then studied by using the same electrochemical technique at room temperature in the potential range of 0.0 to 2.5 V. These measurements were carried out in 0.5 M and 1M H$_2$SO$_4$ solution at the scan rate of 10 mV.s^{-1} which was again optimized by scan rate dependent current density curve (inset Fig. 3b). Fig. 3a shows the polarization curves of the OER study using CZTS nanoparticles from which the maximum current density was found to be 12.65 mA.cm^{-2} for 0.5M H$_2$SO$_4$ and 9.1 mA.cm^{-2} for 1M H$_2$SO$_4$ at an applied potential of 2.50 V. The excellent catalytic stability for OER activity was also observed by CZTS catalyst and has shown only 9.6 % activity degradation after 100 cycles as shown in Fig. 3b. Thus, CZTS could be also used in water oxidation reaction for the evolution of oxygen. The expected oxygen evolution reaction mechanism

followed by hydrophilic CZTS is also based on the adsorption of OH⁻ over bare CZTS surfaces following the reactions as stated below:[33,34]

$$CZTS + H_2O \rightarrow OH_{ads}CZTS + H^+ + e^- \tag{6}$$

$$OH_{ads}CZTS \rightarrow O_{ads}CZTS + H^+ + e^- \tag{7}$$

$$2O_{ads}CZTS \rightarrow O_2 + CZTS + 2e^- \tag{8}$$
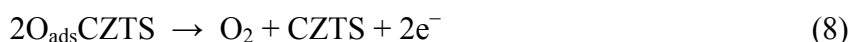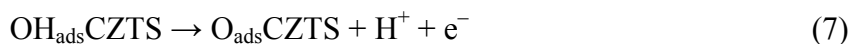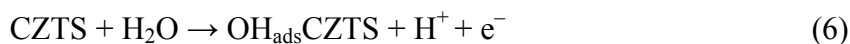
3.2. Photocatalytic Degradation of Dyes

Photocatalytic activity of the as-synthesized hydrophilic CZTS nanoparticles was studied by optical absorption measurements using model dye degradation experiments by determining the relative reduction in the peak intensity of the dye absorption peak against time in the presence of CZTS catalyst under indoor light illumination. 10-25 mg of as-synthesized CZTS was utilized for the degradation of 50 ml of 0.002, 0.004 and 0.01 mM solution of RhB, MB and MR. Several factors as reported earlier have been taken into account during present photocatalytic measurements.[31,35,36]

Fig. 4 demonstrates the results of degradation of RhB by indoor light in presence of CZTS NPs photocatalyst. The optical absorption spectrum of RhB without added CZTS catalyst showed maximum absorption 'λ_{max}' at 554 nm with no accountable change in peak intensity observed over a period of time. However a very large reduction in the peak intensity at λ_{max} was observed within few seconds of addition of hydrophilic CZTS NPs. The complete degradation of 50 ml of 0.004 mM RhB with 25 mg CZTS was observed in just 4 min and the apparent rate constant (k_{app}) was calculated from linear plot of $In[A_t][A_o]$ vs. time for the dye degradation reaction was found to be 0.0186 s⁻¹ (Fig. 4a, b). To further gain insight, effect of concentration of RhB and catalyst loading on rate of reaction was studied keeping other parameters constant (Fig. S3) and found k_{app} depends on the concentration of dye solution and the amount of catalyst loaded. While with decrease of RhB concentration to 0.002 mM keeping the other experimental parameters constant instantaneous degradation of dye occurred just in 10 s with a visible disappearance of pink color (Fig. 4c, e). Unlike the reported degradation time of 4 hr for comparable concentrations of dye with gold nanoparticles decorated CZTS,[3] the exceptionally high value of rate constant and very small time required for degradation of RhB was obtained again and again in the present case in repeated experiments and material was tested and found to be very effective for the photocatalytic degradation with approximately 5% loss in efficiency upto 10 cycles and

~20% loss in efficiency till 25 cycles as shown in Fig. 4d. The pathway followed by photoactive catalyst CZTS under the presence of light is described schematically in Fig. 4.[37]

The gradual decrease in absorption intensity of RhB at λ_{max} with increasing reaction time without any shift of the absorption wavelength suggests no de-ethylation but complete cleavage of RhB chromophores.[38] The rapid degradation of cationic dye RhB points toward interesting interaction between the RhB and hydrophilic CZTS surface. The NPs with small dimensions, 2-4 nm in present case of CZTS are known to have very high surface area and high surface energies, and hence in the absence of any stabilizing agent (such as long chain surfactants) the surface energies of these nanocrystals are majorly balanced by surface adsorbed counter ions present in the reaction medium by electrostatic interactions.[10-15] As the synthesis and photocatalytic reactions were performed in aqueous medium and no chloride elements found under elemental mapping and XPS analyses, the most probable ions present on the CZTS surface could be OH^- ions (a negative surface charge is confirmed by Zeta potential measurement, Fig. S4). Interestingly these surface adsorbed OH^- ions have dual critical role to play in photocatalytic dye degradation of the cationic dyes (RhB and MB) by making the surface of CZTS negatively charged and generation of OH* free radicals by capturing holes from CZTS valence band upon illumination. The cationic dyes have strong electrostatic field interaction with the negatively charged surfaces of CZTS and get rapidly adsorbed over the CZTS surface due to which oxidation of dye molecules over CZTS surface facilitated.[38] The excitons are generated when the photoactive material is exposed to illumination. As the material is visible light active hence, the excitons are generated inside the material upon illumination under indoor light having radiation in the visible region. As shown in Fig. 4e, the electron-hole pair is generated, electron from the valence band of CZTS got transferred to the conduction band of CZTS and the left out hole is taken by surface adsorbed OH^- ion and an OH* is generated which is responsible for the photocatalyzed free radical degradation of RhB in aqueous medium.

The high photocatalytic efficiency of CZTS nanoparticles could be explained by possible presence of quintessential OH^- at the surface of hydrophilic CZTS which can immediately extract the hole from the CZTS valence band and results in rapid generation of large amount of OH* radicals as shown in photocatalytic degradation mechanism (Fig. 4e). Also, in the presence of visible radiation the dye itself works as sensitizer.[38,39] The formation of RhB* (excited RhB state) from RhB ground state by absorption of photons from the visible radiation and the transfer of e^- from RhB to CZTS conduction band leads to increase of

electron population in the CZTS conduction band, however these electron are rapidly extracted by the adsorbed O_2 which ultimately results to the formation of more OH* radicals and enhance the rate of reaction.[40]

The efficiency of CZTS photocatalyst for the degradation of other cationic (Methylene Blue) and neutral (Methyl Red) was also tested and the results are shown in Fig. 5. Excellent photo dye degradation efficiency was observed in case of methylene blue with rate constant (calculated from linear plot of $In[A_t][A_o]$ vs. time) of 0.0031 s^{-1} and dye degradation time of 15 min for 50 ml of 0.004 mM dye with 25 mg of CZTS as shown in Fig. 5a, b. The observed k_{app} for the degradation of 50 ml of 0.002 mM of methyl red with 25 mg of CZTS catalyst was found to be 0.0064 s^{-1} (Fig. 5c, d). Interestingly, in these cases too no observable degradation detected in absence of CZTS catalyst over a period of 2 hr and no shift in peak positions observed under degradation condition. Degradation can be extended to higher concentration of dye (0.01 mM), keeping the amount of catalyst intact without much disturbing the rate of the reaction (Fig. S5). To further clarify the acceptability of surfactant free CZTS NPs and advantage of having negative surface charge (OH^-) for efficient photocatalytic degradation of cationic and neutral dyes, degradation of an anionic dye (Eosin Y) is considered as a case study. Because of the negative surface charge of CZTS NPs catalyst and the anionic nature of Eosin Y dye, a repulsive interaction between the negatively charged CZTS surface and anionic dye molecule is expected. Hence a reduced k_{app} and increase in dye degradation time is resulted as expected from the degradation reaction of this dye (see Fig. S6). However, still there is a possibility of electron transfer from Eosin Y to CZTS conduction band due to polarization of dye molecules with their large skeletal spread outs which could be the possible reason for very good efficiency of CZTS photocatalyst even in case of anionic dyes.[37] At this point it is important to note that, in case of all photocatalytic degradation reactions a very fast and a very slow kinetic part was observed. In all the cases (Fig. 5, Fig. S3, S5, S6) majority of the degradation ca. 80% takes place within 3 min from the addition of CZTS catalyst. Then there is slow down of the reaction to different extended time depending on the dyes. To what extent this behavior is observed could be related to catalyst surface retardation might be due to complete coverage of the catalyst surface with degraded molecules, a slow desorption process as well as nonuse of any type of scavenger during the reactions. Use of a right type scavenger (e.g. ammonium oxalate)[24] should still enhance the rate of the reaction to further extent and even reduce the time of the degradation reaction.

As a controlled reaction, the dye degradation experiments were also performed in dark and one of the representative data for MB degradation in dark is shown in Fig. S7 in ESI. The results from the experiment are concluded as (i) the dye itself does not show any degradation, and (ii) the dye degradation does not occur even in the presence of catalyst under dark. However, a slight reduction in the peak intensity at λ_{max} = 664 nm with time (up to 30 min) was observed under dark which could be attributed to the adsorption of dye on highly hydrophilic nanoparticles. The concentration of dye became constant after 30 min. However, if the dye is exposed to illumination just after the addition of photoactive CZTS, both the adsorption and degradation of dye occurs simultaneously and high degradation rate is observed. Hence, both the catalyst and light are quintessential for photocatalytic dye degradation.

3.3. Photocatalytic Reduction of Chromium (VI)

Apart from hydrogen evolution and dye degradation reactions, the hydrophilic CZTS nanoparticles were found to have effective application in reduction of another water pollutant Cr(VI). The carcinogenic and mutagenic Cr(VI) is driven off in water from various industrial processes such as electroplating and paint making etc. Instead of chemical treatment, photocatalytic reduction of Cr(VI) to non-toxic Cr(III) using photoactive semiconductor is considered as most promising.[41,42] The effective removal of Cr(VI) upto 99.8% was observed in 15 minutes in a 50 ml of Cr(VI) 0.05 mM solution with calculated high rate constant value of 0.0049 s^{-1} utilizing 50 mg of hydrophilic CZTS nanoparticles (Fig. 6). The obtained results are notable without adding any reducing agent such as NaBH$_4$, than those reported earlier with SnS$_2$.[42] A simple mechanism is proposed for the indoor light induced Cr(VI) reduction reaction and the step by step reactions are expressed in Eq. 9-11. Excitons formed due to the light absorption by CZTS semiconductor NPs and the generated electrons from the valence band of CZTS got transferred to the conduction band of CZTS as shown in schematic diagram in Fig. 4e and Eq. 9. Simultaneously the excited electrons are captured by the adsorbed Cr(VI)-complexes present on the surface and as a result, Cr(VI) is reduced to nontoxic Cr(III). A visible color change of the chromium complex solution from light yellow to colorless is observed after the completion of the reaction pertaining the removal of Cr(VI).

$$CZTS + h\nu \rightarrow e^-_{cb} + h^+_{vb} \tag{9}$$

$$Cr(VI)_{ads}CZTS + 3e^-_{cb} \rightarrow Cr(III)_{ads}CZTS \tag{10}$$

$$Cr(III)_{ads}CZTS + Cr(VI) \rightarrow Cr(III) + Cr(VI)_{ads}CZTS \tag{11}$$
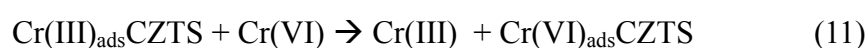
In all the catalytic reactions mentioned above, after the recyclability tests CZTS catalyst samples were recovered and dried. After several continuous and repeated cycles, it is important to know whether the CZTS nanoparticles retain their original properties or not. To check these states of the nanoparticles, XRD, TEM, Raman and optical measurements have been carried out again on the recovered samples and the results are shown in Fig. 7 considering a photocatalytic reaction as case study. It could be clearly ascertain from Fig. 7a that the CZTS nanoparticles retained the original kesterite structure as shown earlier in Fig. 1a even after 10th of catalytic cycles accompanying a slight decrease in peak intensity. Similar retention behavior of particle morphology and absorbance property are observed by comparing Fig. 7b with Fig. 1b,e. However the slight decrease in XRD peak intensity and increase in absorbance at around 600 nm (minor blue shift too) corroborated to the reduction of particle size due to the removal of few surface atoms of CZTS and also might be reason to the adsorption of substrate molecules during repeated catalytic process. The same phenomenon could be reason for the Raman spectra (inset i, Fig. 7b), where shape of the Raman spectra remains similar however $\pm$ 3-5 cm^{-1} shift on peak position. Hence, it is now confirmed that, our as-synthesized Cu_2ZnSnS_4 nanoparticles could be used several times in electrocatalytic and photocatalytic applications without compromising the quality of the particles. Finally XPS measurement has been performed on the CZTS sample to further correlate the electronic effects and the catalytic properties (see Fig. S8 for XPS spectra). All the binding energies and peak splittings of the as-synthesized sample are in good agreement with the values reported earlier for Cu^+, Zn^{2+}, Sn^{4+}, and S^{2-} in Cu_2ZnSnS_4,[14,43] however indicting the absence of Cu^{2+} and Sn^{2+}. Another important feature observed is the appearance of a very strong O 1s peak at 531.2 eV in the full range XPS spectrum demonstrating the presence of surface-adsorbed oxygen, which is in fact essential for the dispersion of the surfactant free CZTS nanoparticles in water and for the photocatalytic degradation reactions as discussed in the above sections.

4. Conclusions

The results displayed the applications of surfactant free Cu_2ZnSnS_4 nanoparticles as efficient three way multifunctional heterogeneous catalyst for hydrogen and oxygen evolution, polluting dye degradation reactions and carcinogenic Cr(VI) removal reactions. The obtained current density values for hydrogen evolution reaction through electrochemical study and exceptionally high rate constant for dye degradation reactions and reduction of Cr(VI) to Cr(III) showed that the surfactant free CZTS nanoparticles are potential candidate

of multifunctional semiconductors for wide range of technological applications considering the promising results and cost economic factors. All the electrocatalytic and photocatalytic applications under indoor light illumination without incorporation of any expensive noble metal, in the absence of any harsh reducing/oxidizing agent and artificial UV radiation is highly efficient and economical, hence we emphasize the application of such surfactant free materials in further technical fields.

CZTS nanocatalysts have been reused for 100 cycles in the water splitting reaction and 25 cycles in the dye degradation and reduction reactions. Further characterization on recovered catalysts after the final cycles clarify the retentivity of original morphology, crystal structure and most importantly optical properties, confirming the repeated use of the our Cu_2ZnSnS_4 NPs without compromising the intrinsic qualities.

Electronic supplementary information (ESI) available: Details TOF calculation, material characterization results by HRTEM and BET, DLS measurement, optical absorption spectra of degradation of dyes at various controlled conditions.

References

1. S. Linic, P. Christopher and D. B. Ingram, *Nat. Mater.* 2011, **10**, 911.

2. X. Zhao and C. Burda, *Energy Environ. Sci.* 2012, **5**, 5564.

3. X. Yu, A. Shavel, X. An, Z. Luo, M. Ibáñez and A. Cabot, *J. Am. Chem. Soc*. 2014, **136**, 9236.

4. J. Gao, H. Gu and B. Xu, *Acc. Chem. Res.* 2009, **42**, 1097.

5. Y. Liu, L. Zhou, Y. Hu, C. Guo, H. Qian, F. Zhanga and X. W. Lou, *J. Mater. Chem.* 2011, **21**, 18359.

6. S. Jana, B. B. Srivastava, S. Jana, R. Bose and N. Pradhan, *J. Phys. Chem. Lett.* 2012, **3**, 2535.

7. Q. N. Xia, Q. Cuan, X.-H. Liu, X.-Q. Gong, G.-Z. Lu and Y.-Q. Wang, *Angew. Chem. Int. Ed.* 2014, **53**, 9755.

8. M. Kumar and S. Deka, *ACS Appl. Mater. Interfaces*, 2014, **6***,* 16071.

9. H. Zhou, W.-C. Hsu, H.-S. Duan, B. Bob, W. Yang, T.-B. Song, C.-J. Hsu and Y. Yang, *Energy Environ. Sci.* 2013, **6**, 2822.

10. F.-J. Fan, L. Wu and S.-H. Yu, *Energy Environ. Sci.* 2014, **7**, 190.

11. J. Wang, P. Zhang, X. Song and L. Gao, *RSC Adv.* 2014, **4**, 27805.

12. L. Rovelli, S. D. Tilley and S. K. Sivula, *ACS Appl. Mater. Interfaces* 2013, **5**, 8018.

13. Z. C. Holman and U. R. Kortshagen, *NanoLett.* 2011, **11**, 2133.

14. P. Kush, S. K. Ujjain, N. C. Mehra, P. Jha, R. K. Sharma and S. Deka, *ChemPhysChem* 2013, **14**, 2793.

15. P. Kush and S. Deka. *J. Nanopart. Res*. 2014, **16**, 2600.

16. D. Merki and X. Hu, *Energy Environ. Sci.* 2011, **4**, 3878.

17. B. Kumar, S. Saha, M. Basu and A. K. Ganguli. *J. Mater. Chem. A* 2013, **1**, 4728.

18. D. Kong, H. Wang, Z. Lu and Y. Cui, *J. Am. Chem. Soc*. 2014, **136**, 4897.

19. M. Grzelczak, J. Zhang, J. Pfrommer, J. Hartmann, M. Driess, M. Antonietti and X. Wang. *ACS Catal*. 2013, **3**, 383.

20. Y. Li, H. Wang, L. Xie, Y. Liang, G. Hong and H. Dai, *J. Am. Chem. Soc*. 2011, **133**, 7296.

21. M. A. Lukowski, A. S. Daniel, F. Meng, A. Forticaux, L. Li and S. Jin, *J. Am. Chem. Soc*. 2013, **135**, 10274.

22. X. Zheng, J. Xu, K. Yan, H. Wang, Z. Wang and S. Yang. *Chem. Mater.* 2014, **26**, 2344.

23. S. S. Dunkle, R. J. Helmich and K. S. Suslick, *J. Phys. Chem. C* 2009, **113**, 11980.

24. S. Kumar, S. Khanchandani, M. Thirumal and A. K. Ganguli, *ACS Appl. Mater. Interfaces* 2014, **6**, 13221.

25. R. Rajesh, S. S. Kumar and R. Venkatesan, *New J. Chem*. 2014, **38**, 1551.

26. U. Soni, P. Tripathy and S. Sapra, *J. Phys. Chem. Lett.*, 2014, **5**, 1909.

27. Y.-P. Tsai, R. Doong, J.-C. Yang and Y.-J. Wu, *J Chem. Technol. Biotechnol.* 2011, **86**, 949.

28. X. Wang, S. O. Pehkonen and A. K. Ray, *Ind. Eng. Chem. Res*. 2004, **43**, 1665.

29. J. Zhang, G. Zhang, M. Wang, K. Zheng, D. Cai and Z. Wu, *Nanoscale* 2013, **5**, 9917.

30. J. M. Buriak, P. V. Kamat and K. S. Schanze, *ACS Appl. Mater. Interfaces* 2014, **6**, 11815.

31. D. Voiry, M. Salehi, R. Silva, T. Fujita, M. Chen, T. Asefa, V. B. Shenoy, G. Eda and M. Chhowalla, *NanoLett*. 2013, **13**, 6222.

32. E. J. Popczun, C. G. Read, C. W. Roske, N. S. Lewis and R. E. Schaak, *Angew. Chem. Int. Ed*. 2014, **53**, 5427.

33. H. B. Suffredini, S. A. S. Machado and L. A. Avaca, *J. Braz. Chem. Soc*. 2004, **15**, 16.

34. R. Subbaraman, D. Tripkovic, K.-C. Chang, D. Strmcnik, A. P. Paulikas, P. Hirunsit, M. Chan, J. Greeley, V. Stamenkovic and N. M. Markovic, *Nat. mater.* 2012, **11**, 550.

35. N. Serpone and A. Salinaro, *Pure Appl. Chem.* 1999, **71**, 303.

36. B. Ohtani, *Phys. Chem. Chem. Phys.* 2014, **16**, 1788.

37. Z. Chen, D. Li, W. Zhang, Y. Shao, T. Chen, M. Sun and X. Fu, *J. Phys. Chem. C* 2009, **113**, 4433.

38. M. Basu, A. K. Sinha, M. Pradhan, S. Sarkar, Y. Negishi, Govind, and T. Pal, *Environ. Sci. Technol*. 2010, **44**, 6313.

39. T. Lv, L. Pan, X. Liu, T. Lu, G. Zhu, Z. Sun and C. Q. Sun, *Catal. Sci. Technol.* 2012, **2**, 754.

40. Z. Xiong, L. L. Zhang, J. Ma and X. S. Zhao, *Chem. Commun.* 2010, **46**, 6099.

41. C. Mondal, M. Ganguly, J. Pal, A. Roy, J. Jana and T. Pal, *Langmuir* 2014, **30**, 4157.

42. Y. C. Zhang, J. Li and M. Zhang, *Environ. Sci. Technol.* 2011, **45**, 9324.

43. A. Singh, H. Geaney, F. Laffir and K. M. Ryan, *J. Am. Chem. Soc.* 2012, **134**, 2910.
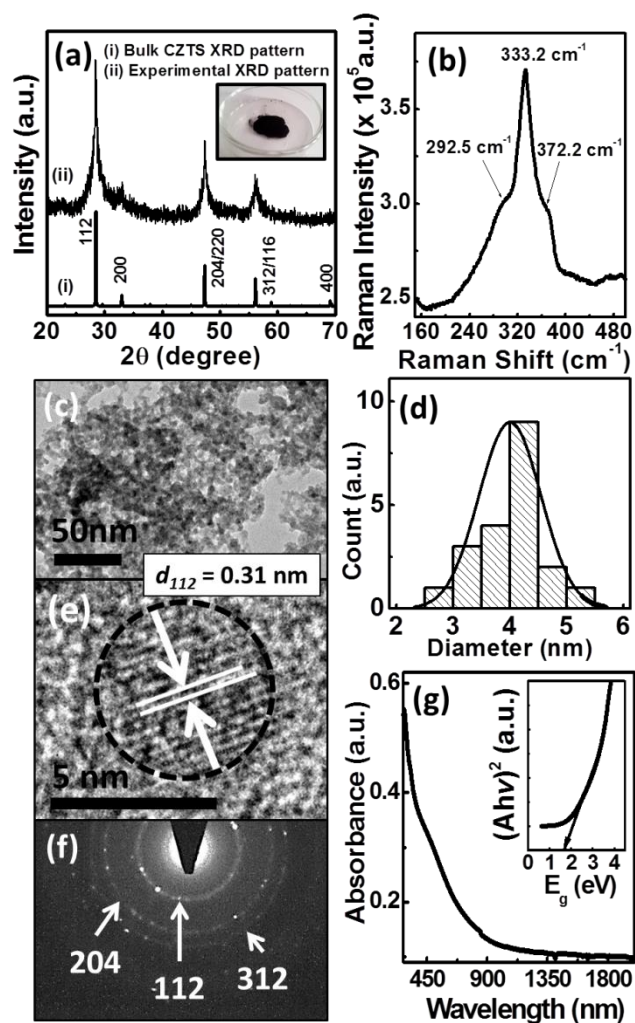
Fig. 1 Characterization results for as-synthesized hydrophilic CZTS nanoparticles (a) Powder XRD pattern (b) Raman spectrum of as-synthesized CZTS (c)TEM image (inset: hydrophilic CZTS ink) (d) Histogram showing particle sized distribution in as-synthesized CZTS.(e) High resolution TEM image (f) Selected area electron diffraction (SAED) pattern and (g) UV-Vis absorption spectrum (inset: calculated band gap, Tauc plot).
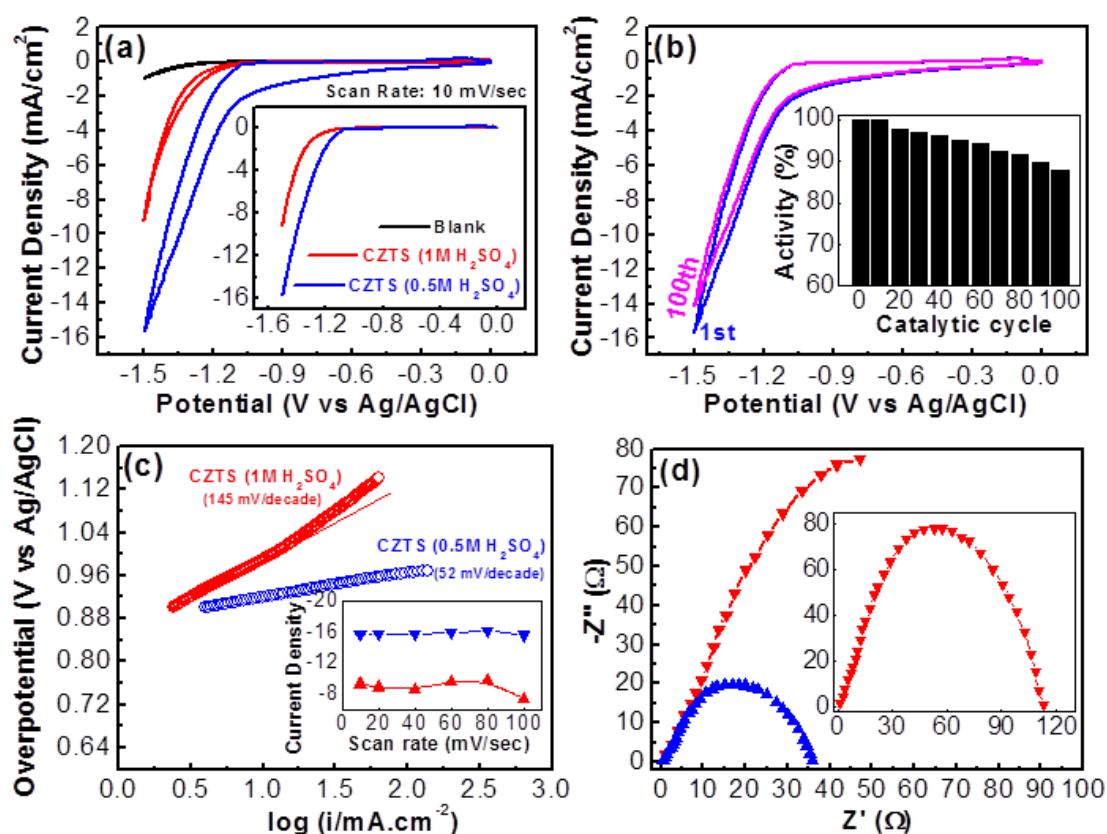
Fig. 2 Electrocatalytic performance of as-synthesized CZTS nanoparticles for HER and OER activity. (a) CV curves of as prepared CZTS electrode in 1M and 0.5M of H$_2$SO$_4$ electrolyte, (inset) corresponding polarization curves obtained from linear sweep voltammetry measurement. (b) CV curves after 1st and 100th catalytic cycle, (inset) normalized catalytic efficiency after various electrochemical cycle, (c) Tafel plots for HER kinetics at different electrolyte concentration, (inset) scan rate dependent current density plots. (d) Nyquist plots showing the facile electrode kinetics of CZTS ink at lower electrolyte concentration.
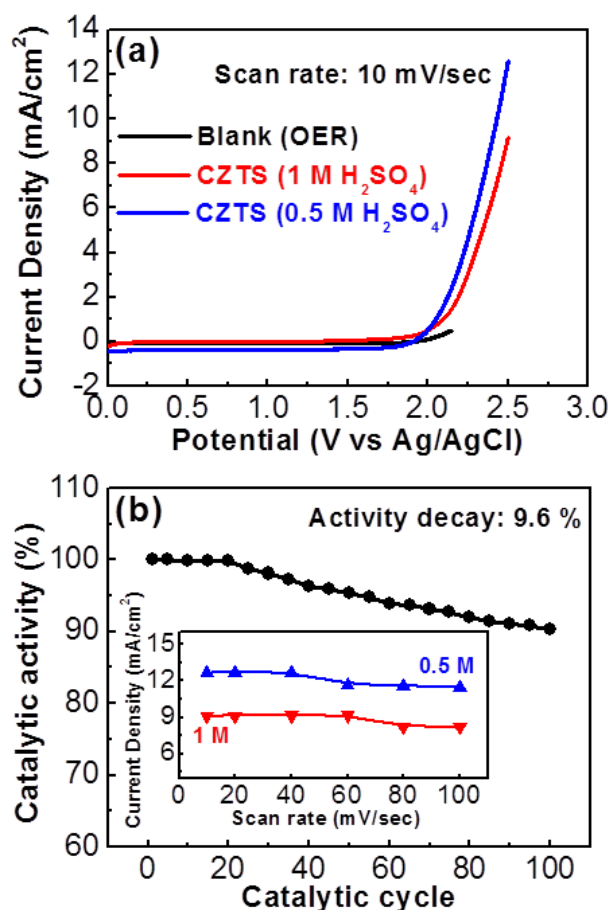
Fig. 3 Electrocatalytic performance of as-synthesized CZTS NPs in OER activity. (a) Polarization curve obtained from linear sweep voltammetry measurement and (b) catalytic activity result showing excellent OER performance after 100 cycles of continuous operation. Inset of 'b' is showing scan rate dependent current density plot.
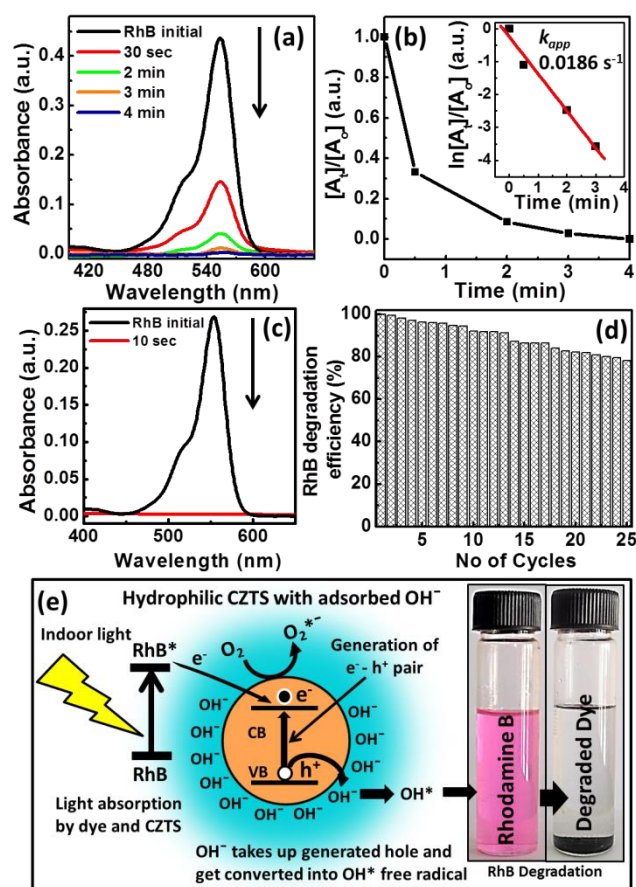
Fig. 4 Optical absorption spectra of (a) 0.004mM, 50 ml RhB by light in presence of 25 mg of CZTS NPs showing degradation of peak intensity at λ_{max} (represented with downward arrow)., (b) plot of $[A_t][A_0]$ vs. reaction time at $\lambda_{max}= 554$ nm, inset: linear plot of $\ln[A_t][A_0]$ vs. time evaluating the rate constant of the RhB degradation reaction. (c) Degradation in absorption peak intensity of RhB at λ_{max} (554 nm) for a 0.002 mM solution in presence of 25 mg catalyst. (d) Recyclability of the CZTS as catalyst for RhB degradation upto 25 cycles from the experiment described in panel 'c', (e) Illustration of possible photocatalytic dye degradation mechanism by surfactant free hydrophilic CZTS.
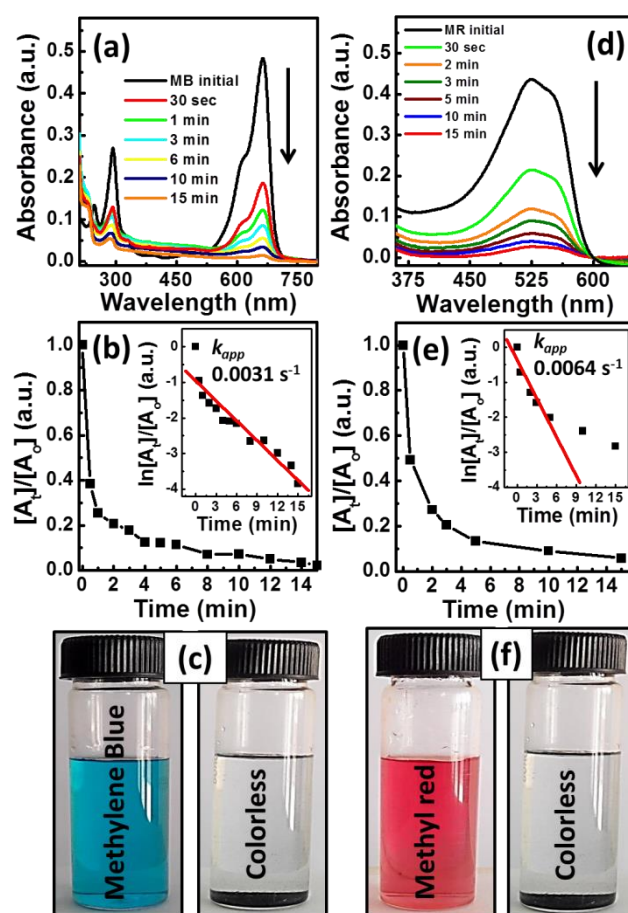
Fig. 5 (a) Optical absorption spectra of 0.004 mM Methylene Blue solution in presence of 25 mg CZTS catalyst showing degradation of peak intensity at λ_{max} (represented with downward arrow) (b) $[A_t][A_0]$ vs. time plot at λ_{max} = 664 nm and inset is the linear plot of $In[A_t][A_0]$ vs. time for first order kinetics. (c,f) change of colour of the dye solution under experiment before and after reaction. (d) Degradation in absorption peak intensity of 0.002 mM aqueous Methyl Red solution at λ_{max} (521 nm) in presence of 25 mg CZTS catalyst (represented with downward arrow) (e) $[A_t][A_0]$ vs. time plot and inset is the $In[A_t][A_0]$ vs. time for first order kinetics.
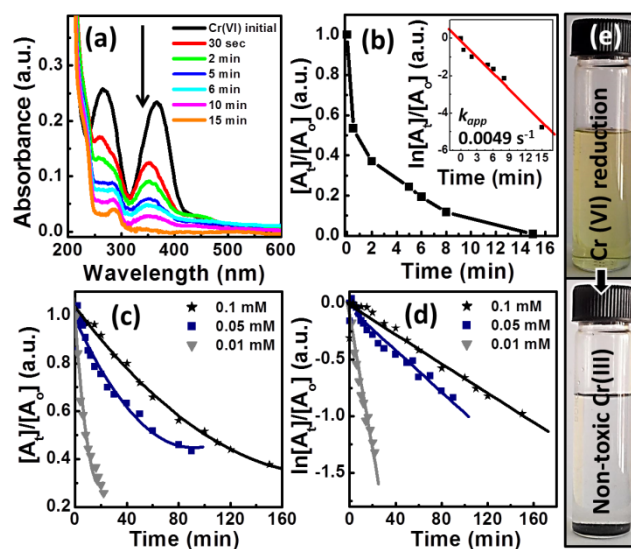
Fig. 6 (a) Optical absorption spectra of 0.05 mM Cr(VI) solution in presence of 50 mg of bare surface CZTS catalyst and absence of any external reducing agent showing degradation of peak intensity at λ_{max} (represented with downward arrow). (b) $[A_t]/[A_0]$ vs. reaction time curve for the same solution from panel 'a', inset: corresponding linear plot of $\ln[A_t][A_0]$ vs. time evaluating the rate constant of the Cr(VI) reduction reaction. (c,d) effect of Cr(VI) concentration on reduction time with 25 mg of CZTS NPs, for a 50 ml of Cr(VI) solution in the concentration range 0.1-0.01 mM. (e) Cr(VI) solutions before and after reduction reaction.
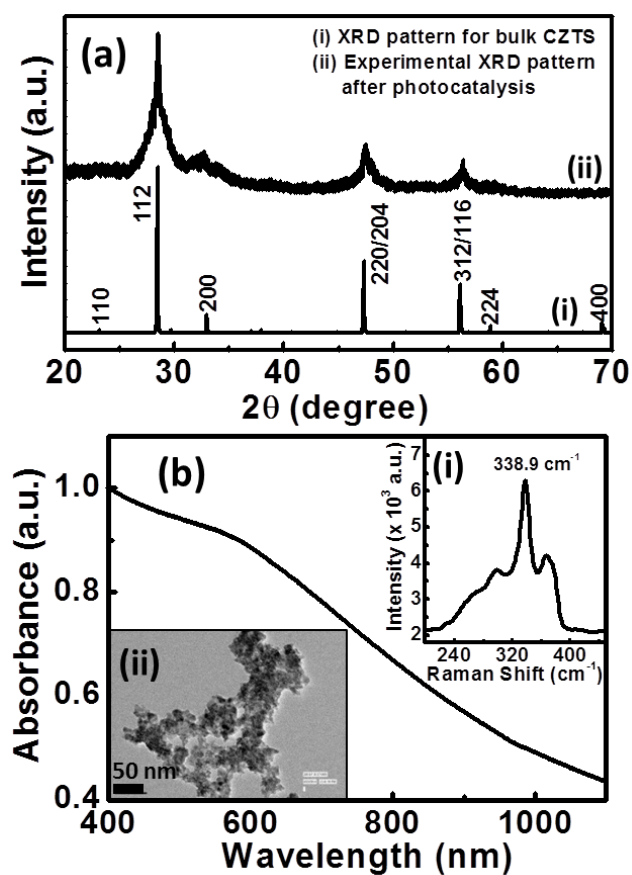
Fig. 7 (a) Bulk XRD pattern of kesterite CZTS (i) and XRD pattern after photocatalysis (ii). (b) Optical absorption spectrum, inset: (i) room temperature Raman spectrum and (ii) TEM image of CZTS nanocatalyst after ten photocatalytic dye degradation cycles.

TABLE OF CONTENT

Use of hydrophilic Cu$_2$ZnSnS$_4$ nanoparticles as Multifunctional Highly Active Heterogeneous Catalyst: Electrocatalytic water splitting, Photocatalytic Dye Degradation and Reduction of Aqueous Cr(VI).